

# Wireless Transfer of Electric Power

by

Robert Alexander Moffatt

Submitted to the Department of Physics  
in partial fulfillment of the requirements for the degree of

Bachelor of Science in Physics


at the

MASSACHUSETTS INSTITUTE OF TECHNOLOGY

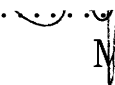
June 2009

© Massachusetts Institute of Technology 2009. All rights reserved.


Author .....

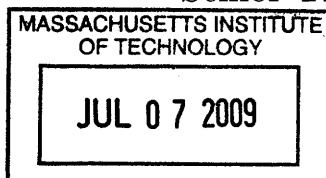
  
Department of Physics  
May 22, 2009

Certified by .....

  
Marin Soljacic  
Assistant Professor of Physics  
Thesis Supervisor

Accepted by .....

  
David Pritchard  
Senior Thesis Coordinator, Department of Physics



**ARCHIVES**



# Wireless Transfer of Electric Power

by

Robert Alexander Moffatt

Submitted to the Department of Physics  
on May 22, 2009, in partial fulfillment of the  
requirements for the degree of  
Bachelor of Science in Physics

## Abstract

In this dissertation, I describe the design and construction of a system which can transfer electric power wirelessly. This is accomplished using inductive, near-field, non-radiative coupling between self-resonant copper helices. In our first experiment, we transferred 60W of power over a distance of 2m with 45% efficiency. In our second experiment, we designed a system which can transfer power from a single source to two devices, each 2m away, with 60% total efficiency. We also developed a quantitative model of our helical resonators which predicted the resonant frequency with an accuracy of 5%.

Thesis Supervisor: Marin Soljagic

Title: Assistant Professor of Physics



## Acknowledgments

I would like to thank all of my collaborators on this project: Andre Kurs, Aristeidis Karalis, Prof. John D. Joannopoulos, Prof. Peter Fisher, and Prof. Marin Soljacic. I would especially like to thank Andre Kurs for the theoretical formulas which he explained and provided, and also for all of the hours he spent with me in the lab completing the final measurements. I am also very grateful to Prof. Marin Soljacic for giving me the opportunity to work on this project. It has been very exciting, and I have greatly enjoyed working with all the members of our group.



# Contents

<b>1</b>	<b>Introduction</b>	<b>13</b>
<b>2</b>	<b>Theory</b>	<b>15</b>
2.1	Coupled-Mode Theory . . . . .	15
2.2	Reflected Impedance . . . . .	17
2.3	Design Schematics . . . . .	18
<b>3</b>	<b>Self-Resonant Helices</b>	<b>21</b>
3.1	Model . . . . .	22
3.2	Losses . . . . .	23
3.3	Coupling . . . . .	23
3.4	Effects of Nearby Objects . . . . .	24
<b>4</b>	<b>Experiment 1</b>	<b>27</b>
4.1	Setup . . . . .	27
4.2	Colpitts Oscillator . . . . .	28
4.3	Coil Q . . . . .	30
4.4	Coupling Constant . . . . .	32
4.5	Efficiency . . . . .	33
<b>5</b>	<b>Experiment 2</b>	<b>35</b>
5.1	Setup . . . . .	35
5.2	Extracting $f_{res}$ , $Q$ , and $k$ from Measurements . . . . .	37
5.3	Tuning and Impedance Matching . . . . .	38
5.4	Efficiency . . . . .	38
5.5	Effects of Parasitic Capacitance . . . . .	39
<b>6</b>	<b>Results 1</b>	<b>41</b>

<b>7 Results 2</b>	<b>43</b>
<b>8 Conclusion</b>	<b>47</b>



# List of Figures

2-1	Coupled Resonators. . . . .	15
2-2	Plot of Efficiency ( $\eta$ ) vs. Strong Coupling Parameter ( $\kappa/\sqrt{\Gamma_1\Gamma_2}$ ). Plot provided by Andre Kurs. . . . .	17
2-3	Reflected Impedance due to mutual inductance, represented by $Z_R$ . . . . .	18
2-4	System design for a single source and a single device. . . . .	18
2-5	System design for a single source and two devices. . . . .	19
3-1	A setup for testing the effects of nearby materials on the coil Q. . . . .	25
4-1	Schematic of the setup for the first experiment. . . . .	27
4-2	Photograph of the setup for measuring power transfer. Our group is standing between the source coil and device coil, obstructing the line-of-sight path. The Colpitts oscillator is to the far left, and the light bulb load is hanging from the device coil on the right. Photo provided by Aristeidis Karalis. . . . .	28
4-3	Colpitts oscillator schematic. . . . .	29
4-4	Photograph of the setup for measuring coil Q. Photo provided by Andre Kurs. . . . .	31
4-5	Photograph of the setup for measuring the coupling constant. Photo provided by Andre Kurs. . . . .	32
5-1	Schematic of the setup for the second experiment. . . . .	35
5-2	Photograph of the setup for the second experiment. Photo taken by the author. . . . .	36
5-3	Diagram of the circuit for the second experiment. . . . .	37
5-4	Schematic depiction of the parasitic capacitances. . . . .	39
6-1	Efficiency as a function of distance between the two coils. . . . .	41
6-2	Coupling constant as a function of distance between the two coils. . . . .	42

6-3	Strong coupling parameter as a function of distance between the two coils. . . . .	42
7-1	Total efficiency of power transfer from source to both devices. . . . .	43
7-2	Efficiency comparison between the two device coils. These measurements were taken between the source and device 1 only, or between the source and device 2 only. . . . .	44
7-3	Q measurements of device and source coils. . . . .	45

# List of Tables

3.1	The Effects of Nearby Objects on Coil Q. . . . .	25
4.1	List of Colpitts Oscillator Parts and Values. . . . .	29
7.1	Total efficiency of power transfer from source to both devices. . . . .	44



# Chapter 1

## Introduction

The goal of this project was to transmit energy from a source to a device without any physical contact between the two, or in other words, without wires. This goal has a long history in electromagnetic research, especially since the discovery and demonstration of effects such as induction, by Faraday, or electromagnetic waves, by Hertz. The most noteworthy researcher in this area was Nicola Tesla, whose goal was to distribute power wirelessly to the entire earth from his Wardencllyffe Tower, perhaps through the excitation of Schumann resonances, although the details of his plan are not entirely clear.

There are many electromagnetic effects which are capable of transferring energy wirelessly from one point to another. The optimal method is determined by the desired distance between the source and device relative to two length scales: (1) the size of the source or device, and (2) the wavelength corresponding to the frequency of oscillation. Short-range transfer takes place over distances much smaller than the size of the source or device, mid-range transfer takes place over distances larger than the source or device, and long-range transfer takes place over distances much larger than the wavelength.

Short-range transfer has been in use for many years and is easily accomplished through the use of induction, as in the case of a transformer. Large amounts of power may be transferred without physical contact, but the coils must be close enough so that the device coil captures a majority of the source coil's magnetic flux. When the distance becomes large, the efficiency drops significantly.

Long-range transfer is usually best accomplished by electromagnetic radiation. Recent attempts at wireless power transmission over long distances have used beams of microwaves directed from the source to the device. This scheme works best for

a stationary source and device, while some sort of tracking mechanism is required if one or the other is in motion. The efficiency of this scheme is determined by the conversion efficiencies of the source and device, and the fraction of microwave power which is lost in transmission.

In the project presented in this dissertation, we sought to design and build a system optimized for mid-range power transfer, i.e. power transfer over a distance several times larger than the device sizes, but shorter than a wavelength. Our system transfers power through the near-field coupling between two electromagnetic resonators. This method has several advantages. (1) Most of the Poynting flux is confined to the near field of the resonators, with a net flow from one resonator to the other. The energy lost by radiation to infinity is relatively small. (2) The near field is non-directional, so there is no need for a tracking mechanism to direct a focused beam from source to device, or an omni-directional radiator which would lose most of its energy to empty space. (3) The source and device may be separated by distances several times their own size while still efficiently transferring power, unlike the case of the transformer.

In the following sections, I describe the theory of operation for our system. Coupled-Mode Theory is explained in detail in a previous publication, [2], so I will only show here the most important results.

# Chapter 2

## Theory

### 2.1 Coupled-Mode Theory

Coupled-mode theory is a method for analyzing the behavior of any number of interacting resonators, such as the example system shown in Figure 2-1. The state of each resonator is described by a complex amplitude which is scaled so that the square of its absolute value is equal to the total energy stored in the resonator. The energy trapped in the system of resonators tunnels between them in a manner analogous to the tunneling of a particle between quantum wells. We also allow each resonator to have a resonant frequency with an imaginary part, which represents a dissipation of power.

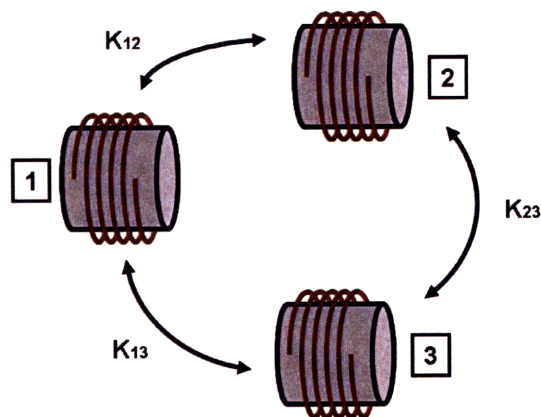


Figure 2-1: Coupled Resonators.

Let  $a_n(t)$  represent the complex amplitude of the  $n$ th resonator. The equation for

the time evolution of  $a_n(t)$  is:

$$\frac{d}{dt} a_n(t) = -i \sum_m K_{nm} a_m(t) + F_n(t) \quad (2.1)$$

where  $F_n(t)$  is an external “force” applied to each resonator. The matrix,  $K_{nm}$ , contains the resonant frequencies along its diagonal, which have the form:  $K_{nn} = \omega_n - i\Gamma_n$ . The off-diagonal terms of  $K_{nm}$  represent the coupling or “tunneling” between the resonators. For more discussion about coupled-mode theory, please refer to the previous publication, [2].

In [3] the efficiency,  $\eta$ , of power transfer from a driven source to a passive device has been calculated to be:

$$\eta = \frac{(\Gamma_W/\Gamma_D)\kappa^2/(\Gamma_S\Gamma_D)}{[1 + \Gamma_W/\Gamma_D]\kappa^2/(\Gamma_S\Gamma_D) + [1 + \Gamma_W/\Gamma_D]^2} \quad (2.2)$$

where  $\kappa$  is the coupling rate,  $\Gamma_S$  is the intrinsic decay rate of the source (due to ohmic loss, radiation, etc.),  $\Gamma_D$  is the intrinsic decay rate of the device, and  $\Gamma_W$  is addition to the intrinsic decay rate of the device due to the load (i.e. the object which is powered wirelessly). Both resonators are assumed to have the same resonant frequency. The efficiency of power transfer is optimized when  $\Gamma_W = \Gamma_D \sqrt{1 + \kappa^2/(\Gamma_S\Gamma_D)}$ . The optimized efficiency is a function only of the strong coupling parameter,  $G$ .

$$\eta = 1 + \frac{2}{G^2} - \frac{2\sqrt{1 + G^2}}{G^2} \quad (2.3)$$

$$G \equiv \kappa/\sqrt{\Gamma_S\Gamma_D} \quad (2.4)$$

Intuitively,  $G$  is the ratio of the rate at which power is transferred to the rate at which power is dissipated. We can see from the plot in Figure 2-2 that the efficiency is large (i.e. greater than 50%) when  $G$  is much larger than 1.

In this research, we also constructed and measured a system with one source and two devices. The formula (provided by Andre Kurs) for the efficiency of a system with one source and two devices is given by:

$$\eta = \frac{x_1(1 + x_2)^2 G_1^2 + x_2(1 + x_1)^2 G_2^2}{(1 + x_1)^2(1 + x_2)^2 + (1 + x_1)(1 + x_2)^2 G_1^2 + (1 + x_2)(1 + x_1)^2 G_2^2} \quad (2.5)$$

where  $G_1$  and  $G_2$  are the strong coupling parameters between the source and devices 1 and 2 respectively, and  $x_1$  and  $x_2$  are the fractional loading of each device, i.e.



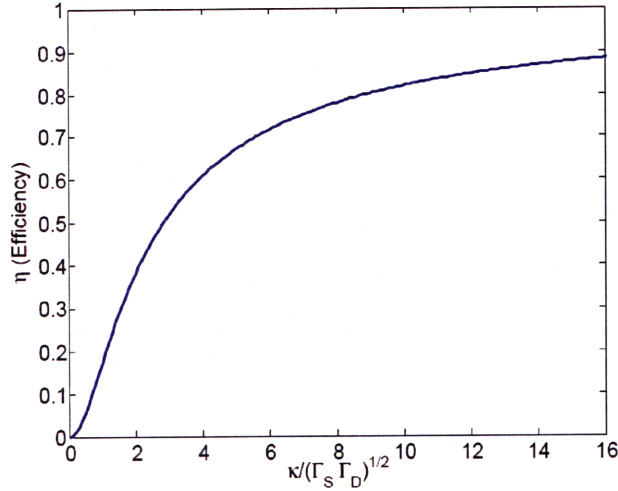


Figure 2-2: Plot of Efficiency ( $\eta$ ) vs. Strong Coupling Parameter ( $\kappa/\sqrt{\Gamma_1\Gamma_2}$ ). Plot provided by Andre Kurs.

$\Gamma_W/\Gamma_D$ . The efficiency is maximized when  $x_1 = x_2 = \sqrt{1 + G_1^2 + G_2^2}$ .

## 2.2 Reflected Impedance

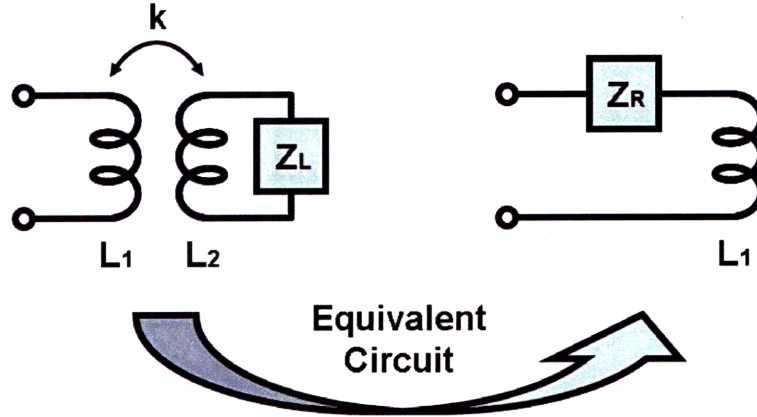
Coupled-mode theory is very general. However, in certain situations it is simpler to analyze a circuit using reflected impedance, which is a lumped-element circuit-theory model which accounts for the effect of mutual inductance. The reflected impedance model works in the following way: Consider the circuit shown on the left in Figure 2-3. We wish to know the input impedance of the inductor,  $L_1$ .

We may analyze this circuit by assuming that  $L_1$  is driven by a sinusoidal current source, with complex amplitude,  $I_1$ , and frequency,  $\omega$ . The induced EMF,  $V_2$ , in  $L_2$  is equal to  $i\omega MI_1$ , where  $M$  is the mutual inductance, and is given by,  $M = k\sqrt{L_1L_2}$ , in terms of the dimensionless coupling constant,  $k$ .

The current flowing through  $L_2$  is given by  $I_2 = V_2/Z_T$ , where  $Z_T$  is the total series impedance of  $L_1$  and  $Z_L$ , and is given by  $Z_T = i\omega L_2 + Z_T$ . The EMF induced back in  $L_1$  by  $I_2$  is given by  $V_1 = -i\omega MI_2$ . This voltage adds to the voltage from the self-inductance of  $L_1$ , and therefore it behaves like a series impedance equal to  $V_1/I_1$ .

Therefore, the circuit may be transformed into the equivalent circuit shown on

Figure 2-3: Reflected Impedance due to mutual inductance, represented by  $Z_R$ .



the right in Figure 2-3. The formula for the reflected impedance is:

$$Z_R = \frac{\omega^2 M^2}{Z_T} = k^2 \frac{\omega L_1 \omega L_2}{Z_T} \quad (2.6)$$

## 2.3 Design Schematics

The following schematic diagrams show the basic elements of the two designs we built and tested. The design shown in Figure 2-4 was used for our first experiment, and consisted of a single source (port 1) and a single device (port 2). Impedance matching was accomplished by varying  $k_s$  and  $k_d$ . The value of  $k$  is set by the separation between the two resonators. In our experiment, we placed the resonators at varying distances, optimized the impedance matching for each distance, and measured the efficiency.

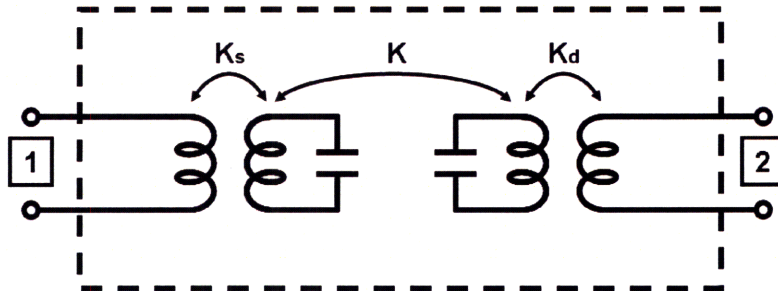


Figure 2-4: System design for a single source and a single device.

The design shown in Figure 2-5 was used for our second experiment, and consisted of a single source (port 1) and two devices (ports 2 and 3). As in the first experiment,

impedance matching was accomplished by varying  $k_s$ ,  $k_{d1}$ , and  $k_{d2}$ . We varied the distance between the resonators, optimized the impedance matching for each distance, and measured the efficiency.

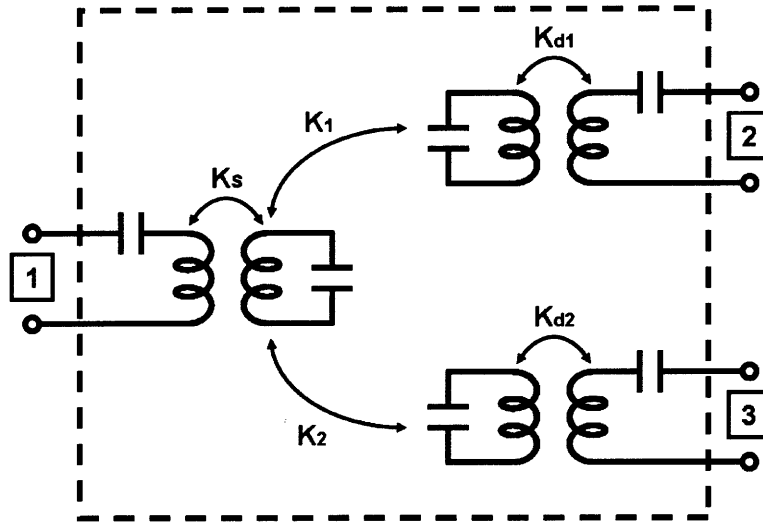


Figure 2-5: System design for a single source and two devices.



# Chapter 3

## Self-Resonant Helices

For our experiments, we decided to use self-resonant helices as our resonators. These consisted of copper pipe wound in a helix shape around a Styrofoam support structure. The copper helix acts as an inductor, and the distributed capacitance across the inductor causes it to behave like an LC resonator. In our experiment, we initially tried several different resonator designs, such as lumped-element LC resonators, but we found the self-resonant helices to have several advantages.

First, the resonators carry oscillating currents on the order of 10A and oscillating voltages on the order of 1000V when transferring powers in the range of 60W. The only available capacitors we could find which could carry high currents and withstand such high voltage with low loss were vacuum capacitors, which unfortunately were bulky, heavy, and expensive.

Second, the fact that the resonator consists of a single piece of continuous copper pipe with no contacts or solder connections allows it to have an exceptionally high Q.

In order to get a rough estimate of the length of pipe necessary to achieve a desired resonant frequency, we used the source, [5], which provides a theoretical treatment of an infinitely long Tesla Coil. One of the findings of this paper was that the wave velocity along the direction of the axis was approximately  $c \sin \psi$ , where  $\psi$  is the pitch angle of the winding, or in other words, the waves behaved almost as if they followed the wire on its helical path around the coil axis while traveling at the speed of light.

Therefore, the resonant frequency of a helical resonator is, to a good approximation, independent of its length or diameter as long as the total length of the wire is held fixed. For the lowest mode of oscillation, the coil will oscillate at the frequency for which the total length of wire is approximately a half-wavelength. This simple model was used to get an order-of-magnitude estimate of the necessary coil length. To

predict the resonant frequency more accurately, we developed a more detailed model, described in the next section.

Once we constructed our coils, we needed to match their resonant frequencies as precisely as possible. In order to fine-tune the frequencies of our resonators, we cut excess copper, stretched or compressed the helix lengthwise, and slid a piece of copper tape closer or farther away in order to increase or decrease the self-capacitance.

One disadvantage which we discovered was the fact that self-resonant helices interact with their surroundings much more strongly than single-turn LC resonators. This difference in behavior is caused by a difference in the electric field structures around the devices. The electric field of the single-turn LC resonator is contained mainly inside the vacuum capacitor, while the electric field of the helical resonator is distributed nearly evenly throughout the space surrounding the device, and may be approximated as a dipole field at distances far from the helix.

Because most environmental objects interact primarily with the electric field, the distributed field of the helical resonator causes stronger interactions than the more confined field of the lumped-element LC resonator.

### 3.1 Model

The most reliable way to predict the behavior of one of our helical resonators would be a finite-element numerical simulation. However, full numerical simulations are very computationally intensive. Therefore, we decided to develop a faster model for predicting resonator behavior based on some simplifying assumptions. I will summarize the main points of this model here. Our previous publication, [2], describes this model in more detail, as does [3].

First, we approximated the current profile along the helix with a sinusoid which had zeros at both open ends and a maximum in the middle. If  $s$  is a parameter which represents the distance along the helix from the center point, and  $l$  is the total length of the helix, then the current has the form,  $I_p \cos(\pi s/l)$ . By the law of conservation of charge,  $d\lambda/dt = -dI/ds$ , the linear charge density must have the form,  $\lambda_p \sin(\pi s/l)$ .

If we define the parameter,  $Q_p$ , to be the integrated total charge on one half of the coil, then we can describe any charge and current distribution on the coil using only two parameters:  $I_p$  and  $Q_p$ . Next, given a charge and current distribution, we can calculate the stored electromagnetic energy. This energy will be quadratic in  $I_p$  and  $Q_p$ . We can use the coefficients of these two terms to define an effective inductance

and capacitance:

$$E = \frac{1}{2}L I_p^2 + \frac{1}{2C} Q_p^2 \quad (3.1)$$

Once we have the effective inductance and capacitance, we can treat the resonator like a lumped-element LC circuit, which gives us the resonant frequency:  $\omega_0 = 1/\sqrt{LC}$ . We can also model the resonator using coupled mode theory by rescaling  $I_p$  and  $Q_p$  so that they respectively become the real and imaginary parts of the complex amplitude,  $a$ .

## 3.2 Losses

There are two main sources of power loss in a helical resonator: (1) ohmic resistance, and (2) radiation, both of which we calculated using our model. The resistive power loss can be calculated by assuming the current is uniformly distributed around the circumference of the copper pipe, varies sinusoidally along its length, and penetrates into the copper by one skin depth (on the order of micrometers at MHz frequencies). The radiative power loss was calculated by determining the radiation field created by the coil's oscillating magnetic and electric dipole moments.

For a helix of  $n$  turns, with wire radius  $a$ , helix radius  $r$ , height  $h$ , wire length  $l$ , and conductivity  $\sigma$ , our calculation showed that the ohmic resistance ( $R_o$ ) and the radiation resistance ( $R_r$ ) are given by: [2], [3]

$$R_o = \sqrt{\frac{\mu_0 \omega}{2\sigma}} \frac{l}{4\pi a} \quad (3.2)$$

$$R_r = \sqrt{\frac{\mu_0}{\epsilon_0}} \left[ \frac{\pi}{12} n^2 \left( \frac{\omega r}{c} \right)^4 + \frac{2}{3\pi^3} \left( \frac{\omega h}{c} \right)^2 \right] \quad (3.3)$$

Using these resistance values, the decay constant is given by  $\Gamma = (R_o + R_r)/(2L)$ , and the quality factor is given by  $Q = \omega_0/(2\Gamma)$ .

## 3.3 Coupling

We calculated the coupling coefficient between two resonators by calculating the power transfer from one resonator to another. This was calculated by performing the inte-

gral: [2]

$$P_{DS} = \int d^3\vec{r} \vec{E}_S \cdot \vec{J}_D \quad (3.4)$$

which gives the power transferred from the source coil to the device coil. We determine the effective mutual impedance from the formula:  $P_{DS} = -i\omega M I_S I_D$ , and the coupling constant,  $\kappa$ , is given by  $\kappa = \omega M / (2\sqrt{L_S L_D})$ . When the separation between the two coils is much greater than their size,  $\kappa$  decreases like  $D^{-3}$ , where  $D$  is their separation, which is the expected behavior of a dipole-dipole interaction.

Using these results, we determined that the optimal frequency range for coils of the size we were considering to be between 1 and 50MHz. This frequency range optimizes the tradeoff between resistive and radiative losses.

### 3.4 Effects of Nearby Objects

In addition to resistive and radiative losses, our helical resonators also experience losses due to interaction with nearby materials. In order to determine which materials had the strongest effect on our coil at 10MHz, we hung an isolated copper helix in mid-air from one of our light fixtures using a piece of waxed string. It was well separated on all sides from any other objects in the room. The resonator consisted of 11 turns of 3mm radius copper pipe wound in a helix with a 34cm diameter and a length of 28cm. Figure 3-1 shows the setup used to measure the Q of this test coil.

Table 3.1 shows the resonant frequency and Q of the test coil when various objects were placed near or inside it. We found that the material with the lowest interaction was Styrofoam, which is likely because Styrofoam is mostly air. Therefore, after this test, we decided to use Styrofoam for all subsequent coil supports and structures.

We also noticed that there were shifts in Q and  $f_{res}$  even when measuring the same setup: See ‘Isolated with Air inside’, tests 1 and 2 in Table 3.1. We presume this may have been caused by a shift in the positioning of the turns of the coil as materials were taken in and out.

The method we used for measuring Q and  $f_{res}$  is described later in section 3.1.3.



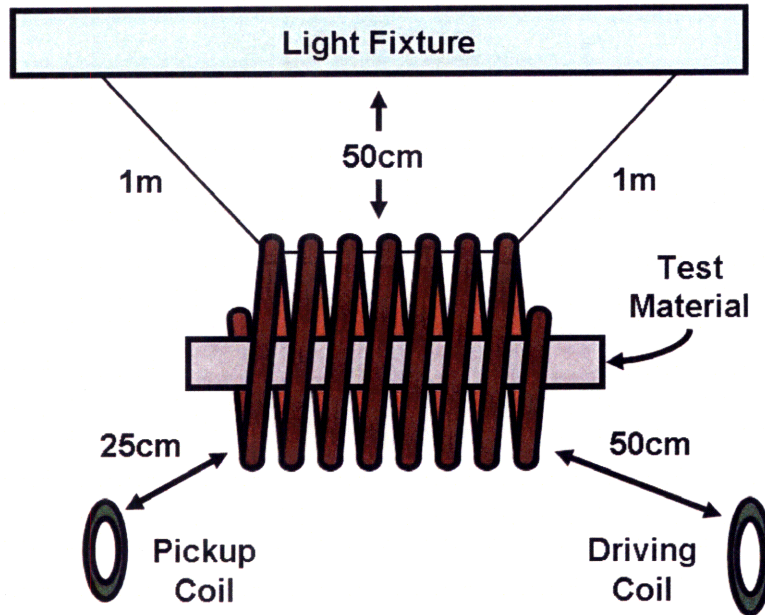


Figure 3-1: A setup for testing the effects of nearby materials on the coil Q.

Table 3.1: The Effects of Nearby Objects on Coil Q.

Test	$f_{res}$ (MHz)	Q
Isolated with Air inside (test 1)	10.5955	1700
Isolated with Styrofoam inside	10.5979	1700
Hand 30cm from Helix w/ Styrofoam	10.5973	1500
Steel chair 30cm from Helix w/ Styrofoam	10.5957	1700
Isolated with Air inside (test 2)	10.4338	1800
Isolated with Cardboard inside	10.3380	590
Isolated with dark PVC inside	10.2770	730
1 inch from wooden box	10.5250	480
4 inches from wooden box	10.6082	1200
5 strips of Scotch tape on surface	10.4744	1870
5 strips of electrical tape on surface	10.3288	1840



# Chapter 4

## Experiment 1

### 4.1 Setup

The setup we used for our first experiment is shown in schematic form in Figure 4-1. Figure 4-2 shows a photograph of our setup with our team posed in front of it. The basic layout consists of two resonators: a source and a device. The source coil is inductively coupled to a Colpitts oscillator circuit, which gets power directly from a standard 60Hz, 120VAC wall outlet. The device coil is inductively coupled to the load, which consists of several turns of wire connected directly to a light bulb.

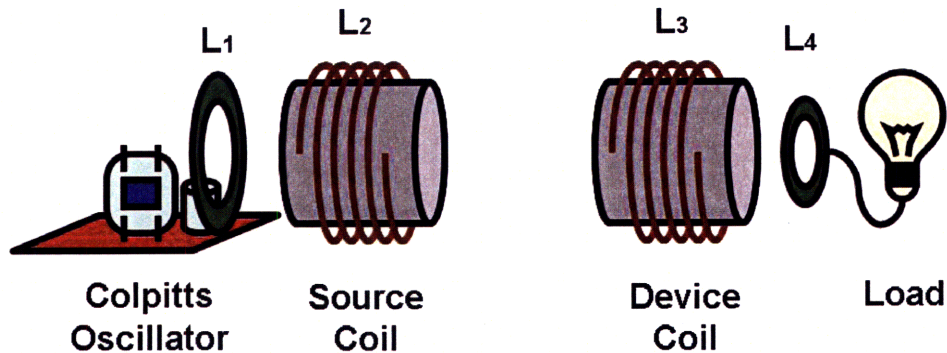


Figure 4-1: Schematic of the setup for the first experiment.

By adjusting the inductive coupling between the oscillator and the source coil and between the device coil and the load, we were able to perform impedance matching and achieve the optimal power transmission efficiency. Also, the two resonators were fine-tuned to resonance with each other by means of extra capacitance from nearby sheets of aluminum foil.

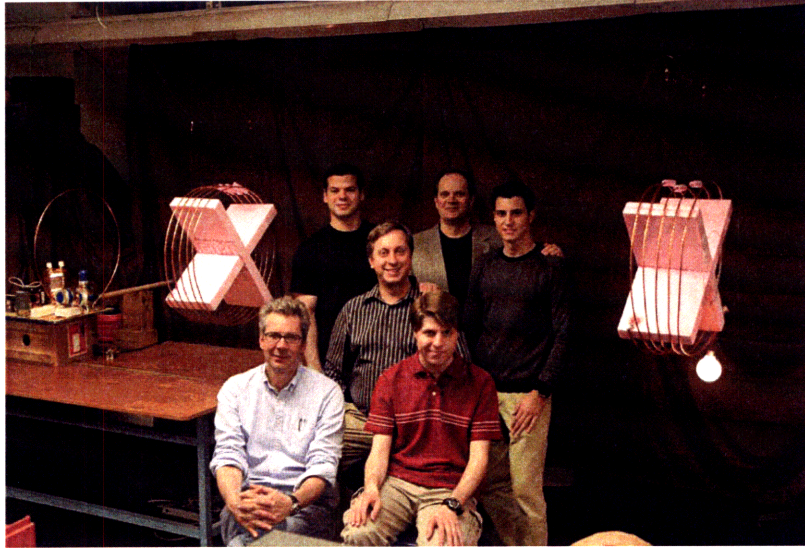


Figure 4-2: Photograph of the setup for measuring power transfer. Our group is standing between the source coil and device coil, obstructing the line-of-sight path. The Colpitts oscillator is to the far left, and the light bulb load is hanging from the device coil on the right. Photo provided by Aristeidis Karalis.

The resonators were made to be as nearly identical as possible. The design parameters are: Wire radius ( $a$ ) = 3mm, Helix radius ( $r$ ) = 30cm, Helix height ( $h$ ) = 20cm, Number of turns ( $n$ ) = 5.25.

As shown in the photo, the resonators were suspended from the ceiling with fishing line in order to minimize their interaction with any other nearby conductors or magnetic materials which could potentially detune them or decrease the  $Q$ . We made sure to keep the space around the coils clear while taking measurements. However, it is interesting to note that the system still worked quite well even when our entire team was standing between the source and device, as demonstrated by the glowing light bulb on the right in Figure 4-2.

## 4.2 Colpitts Oscillator

The schematic for the Colpitts Oscillator is shown in Figure 4-3. The circuit consists of three main pieces: (1) the voltage doubler and power supply, (2) the LC tank circuit, and (3) the Class-C amplifier and feedback circuit. Table 4.1 lists all of the circuit components and their values.

TX1 steps 120VAC up to 2kVAC, and the components  $C_d$ ,  $D_d$ , and  $C_{RF}$ , form

Figure 4-3: Colpitts oscillator schematic.

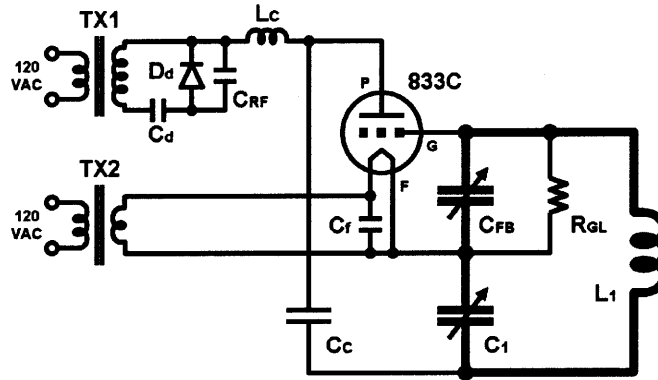


Table 4.1: List of Colpitts Oscillator Parts and Values.

Part	Description	Value
$C_d$	Doubling Capacitor	$1\mu\text{F}$ , 2kV
$D_d$	Doubling Diode	6kV, 100mA
TX1	HV Transformer	2kV, 0.5A
TX2	Filament Transformer	10V, 10A
$C_{RF}$	RF Bypass	10nF, 4kV
$C_f$	Filament Capacitor	1nF, 200V
$L_C$	RF Choke	100 turns, 5cm diam. 5cm long
$C_C$	RF Coupling Capacitor	1nF, 4kV
$L_1$	Tank Circuit Inductor	3/8 in. pipe diam. 60cm loop diam.
$C_1$	Tank Circuit Capacitor	0-500pF Vacuum, set to 200pF
$C_{FB}$	Feedback Capacitor	0-5000pF Vacuum, set to 3000pF
$R_{GL}$	Grid Leak Resistor	10k $\Omega$ , 10W
833C	HV Power Triode	4kV, 500W dissipation

a voltage doubler circuit which supplies 4kV peak to the plate (P) of the 833C. (Because our circuit lacked a sufficiently large smoothing capacitor, the output is a 2kVAC signal superposed on a 2kVDC signal. For the purposes of RF design, 60Hz may be treated as DC.)  $C_{RF}$  filters out any RF fluctuations to produce a smooth 4kV supply voltage.  $L_c$  acts as an open circuit to RF signals, and  $C_C$  acts as an RF short.

$L_1$ ,  $C_1$ , and  $C_{FB}$  form the resonant tank circuit. This circuit carries tens of amps of oscillating current at full power, so all wires need to be thick, and are shown in bold in the schematic. The oscillation frequency is set by the combination of inductance and capacitance in the tank circuit, and we tuned the circuit by varying  $C_1$ .

The pair of capacitors,  $C_1$ , and  $C_{FB}$ , act as a capacitive voltage divider, and the

voltage from the 833C grid (G) to filament (F) is set to about 1/16 of the total voltage across  $C_1$ , and  $C_{FB}$ . (Note that, in order for oscillation to occur, the voltage division ratio must be larger than 1 divided by the triode amplification factor, which is 35 in the case of the 833C.) The grid voltage controls the plate current, which consists of an RF component superposed on a constant DC value. When the plate draws RF current, it cannot flow through  $L_c$ , so it must flow through  $C_C$ , and is therefore drawn from  $C_1$ . The polarity of the voltages and currents are such that this adds energy to the oscillations in the tank circuit, increasing their amplitude. The amplitude of the oscillations grows exponentially until it reaches a magnitude close to the plate supply voltage and the tube becomes nonlinear. The oscillations then level off to a steady state amplitude near this value.

During part of the RF cycle, some current is drawn by the grid, which behaves like a diode. This current flows through  $R_{GL}$ , and  $C_{FB}$  filters this signal to produce a negative DC bias on the grid. This negative bias causes the 833C to work as a Class-C amplifier, and the size of this bias determines the amount of power added to the tank circuit during each cycle. There is a tradeoff between power and efficiency, and a compromise can be chosen by varying the resistance of  $R_{GL}$ . We tried several different values, and we found that  $10\text{k}\Omega$  worked well for our application.

Finally, we controlled the oscillation amplitude by running TX1 from a variac. In this way, we could continuously vary the plate supply voltage, and therefore the oscillation amplitude as well.

### 4.3 Coil Q

Figure 4-4 shows a photograph of the system we used for measuring the Q of our resonators. We used a function generator connected to a small coil to excite oscillations in the resonator. These oscillations were detected by a pickup coil which was connected to an oscilloscope. Both the excitation and pickup coils were placed as far as possible from the resonator in order to minimize any extraneous loading on the resonator from parasitic capacitance or any other undesired effects.

We extracted the Q from the resonance behavior in the following way: The response of a resonator with resonant frequency,  $\omega_0$ , and decay constant,  $\Gamma$ , to a sinusoidal driving EMF,  $F e^{-i\omega t}$ , is given by:

$$a(t) = \frac{F e^{-i\omega t}}{i(\omega_0 - \omega) + \Gamma} \quad (4.1)$$

The free oscillations of a damped resonator take the form of a decaying exponential:

$$a(t) = a_0 e^{-i\omega_0 t} e^{-\Gamma t} \quad (4.2)$$

The quality factor,  $Q$ , is given by:

$$Q \equiv 2\pi \frac{\text{Energy stored}}{\text{Energy lost per cycle}} = 2\pi \frac{|a|^2}{2\Gamma |a|^2 (2\pi/\omega_0)} = \frac{\omega_0}{2\Gamma} \quad (4.3)$$



Figure 4-4: Photograph of the setup for measuring coil  $Q$ . Photo provided by Andre Kurs.

Using this formula for  $Q$ , we can rewrite the steady-state amplitude above as:

$$|a| = F \frac{1}{\sqrt{(\frac{1}{2Q})^2 + (\frac{\delta f}{f_0})^2}}, \quad \delta f \equiv f - f_0 \quad (4.4)$$

Therefore, the amplitude decreases by a factor of  $\sqrt{2}$  when  $|\delta f/f_0| = 1/(2Q)$ . If we define the full-width at  $1/\sqrt{2}$  maximum to be  $\Delta f$ , then  $Q$  is given by:

$$Q = \frac{f_0}{\Delta f} \quad (4.5)$$

This equation allowed us to determine the  $Q$  of a resonator by measuring the width of its response curve. We assumed that the coupling between the resonator and the excitation coil was small enough that any back-reaction of the resonator on the excitation coil would be negligible. Likewise, we assumed that the loading of the resonator by the pickup coil was also negligible. By measuring the full-width at  $1/\sqrt{2}$  maximum of the response curve, we were able to determine the resonator  $Q$  with an accuracy of about 5%.

## 4.4 Coupling Constant

Two coupled resonators have two normal modes of oscillation with two separate resonant frequencies. The lower-frequency mode occurs when the two resonators are in phase, while the higher-frequency mode occurs when they are  $180^\circ$  out of phase. When the two coils have identical resonant frequencies and  $Q$ , the normal mode frequencies occur at:  $\omega_1 = \omega_0 - i\Gamma - \kappa$  and  $\omega_2 = \omega_0 - i\Gamma + \kappa$ . [3]

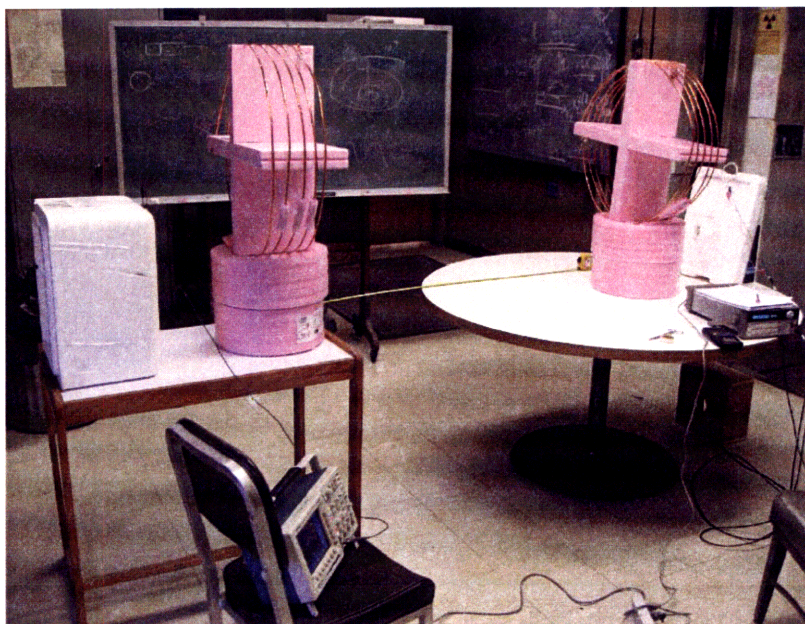


Figure 4-5: Photograph of the setup for measuring the coupling constant. Photo provided by Andre Kurs.

When the system is driven with a sinusoidal signal, there will be two peaks of the frequency response close to the two normal mode frequencies. Using coupled mode



theory, we calculated the frequency splitting for two identical resonators to be: [3]

$$\omega_2 - \omega_1 = 2\sqrt{\kappa^2 - \Gamma^2} \quad (4.6)$$

Therefore, once  $\Gamma$  is known,  $\kappa$  may be calculated from the frequency splitting. Note that this technique only works when  $\kappa$  is larger than  $\Gamma$ . If  $\Gamma$  is too large, there will only be one peak.

In order to measure the frequency splitting, we used a setup similar to that used for Q measurements, except we measured a pair of resonators rather than a single resonator. Figure 4-5 shows the setup we used to measure the coupling constant.

## 4.5 Efficiency

In order to measure the efficiency, we needed a method to measure the power dissipated in each part of our circuit. First, we developed a method for measuring the power dissipated in the load (light bulb) using its brightness, because any oscilloscope connections would detune the circuit, and the extra reactances of the probes could introduce phase errors into voltage and current measurements. Therefore, we used two identical light bulbs: one driven by 120VAC and the other powered wirelessly. We varied the Colpitts oscillator power with a variac until the brightness of the two bulbs matched. Through previous calibrations, we determined that we could determine the light bulb powers to an accuracy of 5%.

Our main concern in this research was to measure the efficiency of the wireless power transfer system. However, we could not simply measure the input power to the Colpitts oscillator because the oscillator circuit is far from 100% efficient. This extra inefficiency posed a problem, because we were interested in designing an efficient system of power transfer, not an efficient Colpitts oscillator.

Therefore, we decided to measure the efficiency using current probes placed on the midpoint of each resonator coil. Using our knowledge of the Q of each resonator, we could determine how much power each of them was dissipating: [2]

$$P_{S,D} = \Gamma L |I_{S,D}|^2 \quad (4.7)$$

$P_S$  and  $P_D$  are the powers dissipated in the source and device coils respectively. The

efficiency of our system is given by the equation:

$$\eta = \frac{P_W}{P_S + P_D + P_W} \quad (4.8)$$

where  $P_W$  is the power dissipated in our calibrated light bulb.

As an extra check, we also measured the input power to the Colpitts oscillator. The wall-to-load efficiency was observed to be about 15%, which gives a lower bound on the efficiency of our wireless power transfer system.

# Chapter 5

## Experiment 2

### 5.1 Setup

The measurements in our second experiment were greatly facilitated by the use of a network analyzer, which was not available at the time we conducted our first experiment. Also, for our second experiment, we decided to transfer power from a single source to two devices. We decided to decrease the device coil size and compensate for this by increasing the source coil size. A schematic of the setup for our second experiment is shown in Figure 5-1, and Figure 5-2 shows a photograph.

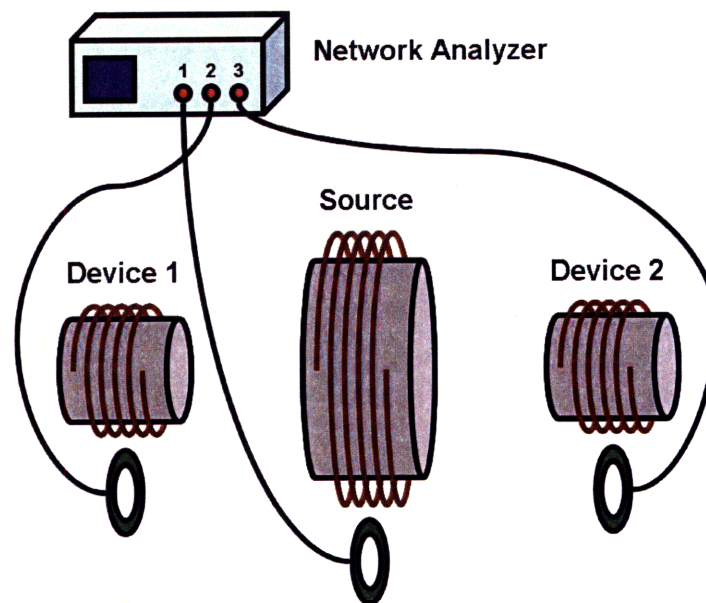


Figure 5-1: Schematic of the setup for the second experiment.

The source coil was 114cm in diameter and consisted of 4 1/8 turns of 12 mm diameter copper pipe. The two device coils were 30cm in diameter and consisted of about 15 turns of 6mm diameter copper pipe. The resonators were all tuned to 6.5MHz using strips of copper foil to vary the self-capacitance. The efficiency was determined by the network analyzer which we used to measure the scattering parameters for a range of separations between the source and device coils.

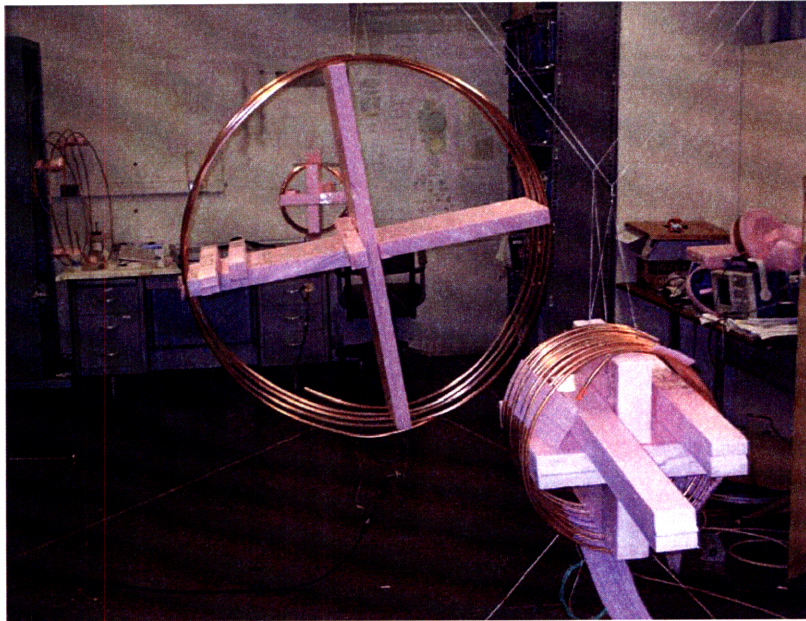


Figure 5-2: Photograph of the setup for the second experiment. Photo taken by the author.

Impedance matching was provided by small LC resonators, which we called “excitation coils”. These were inductively coupled to each of the helical resonators, and they were all tuned to 6.5MHz. (Tuning was not very critical because the excitation coils had Q’s on the order of 100, while the resonators had Q’s on the order of 1000.) Impedance matching was achieved by varying the distance between each helical resonator and its excitation coil. A BNC connector was placed in series with the inductor and variable capacitor and connected to a length of 50 Ohm coaxial cable. The other end of the cable was connected to a port of the network analyzer.

Our network analyzer had four ports and was capable of measuring 1, 2, 3, or 4 port scattering parameters. We selected the 3-port setting. The network analyzer was calibrated with the coaxial cables in place on each of the three ports so that any effects from non-ideal behavior of the cables were accounted for in the calibration. We

used shorts, open circuits, 50 Ohm loads, and direct connections between the ends of the cables in order to perform the calibration.

## 5.2 Extracting $f_{res}$ , $Q$ , and $k$ from Measurements

Figure 5-3 shows a schematic depiction of the circuit for the second experiment. The resonators are represented by lumped-element LC models. The behavior of the system was analyzed using the reflected impedance method. First, 50Ω loads were placed on the output of each device. Next, the load impedance was reflected into each device resonator. Each device impedance was then reflected into the source resonator and added in series. Finally the source impedance was reflected into the source excitation coil.

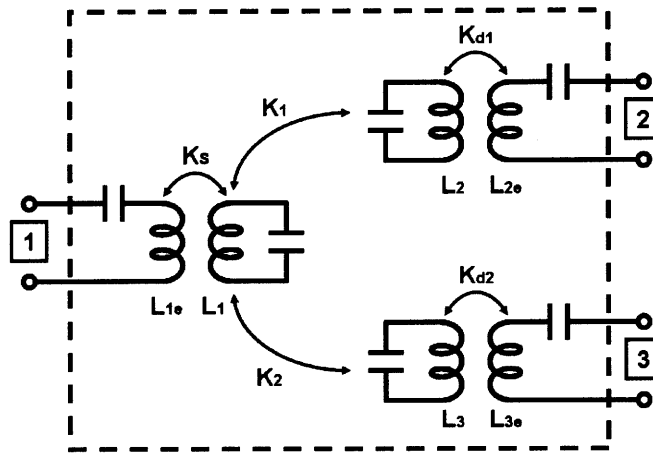


Figure 5-3: Diagram of the circuit for the second experiment.

At each stage of the wireless power transmission, some power is dissipated in the intrinsic resistance of the resonator and some is dissipated in the resistance reflected from the next resonator. The power dissipated in the intrinsic resistance is lost, while the power dissipated in the reflected resistance is transferred to the next resonator. The overall efficiency is equal to the product of the efficiencies of each stage of transmission.

We were able to extract all of the necessary parameters in the following way. First, we shorted all of the resonators which effectively removed them from the circuit. Next we measured the input impedance of the excitation coil,  $L_{1e}$ , as a function

of frequency. By performing a curve fit in Matlab, we were able to determine the inductance, capacitance,  $Q$  and  $f_{res}$  of the excitation coil.

Once we had these parameters, we unshorted  $L_1$  and measured the input impedance of  $L_{1e}$  again. We subtracted the previously measured impedance from this measurement, which left only the reflected impedance from the  $L_1$  resonator. The equation for the reflected impedance is:

$$Z_R = \omega L_{1e} \frac{k_s^2 u^2}{i(u^2 - 1) + u/Q} \quad , \quad u \equiv \omega/\omega_1 \quad (5.1)$$

A Matlab curve fit to this data yielded the  $Q$ ,  $f_{res}$ , and  $k_s$ .

In this way, we were able to measure the  $Q$  and resonant frequencies of all of the resonators and excitation coils, as well as the coupling coefficients between each resonator and its excitation coil. Once these parameters were known, we unshorted  $L_1$  and  $L_2$ , while  $L_3$  remained shorted, and we measured the input impedance of  $L_{1e}$  again. A Matlab curve fit for this plot yielded the value of  $k_1$ . The remaining coupling constants were measured in the same way.

### 5.3 Tuning and Impedance Matching

Once we extracted all of the relevant parameters from our measurements, we used the reflected impedance method to calculate the scattering parameters and the apparent input impedances for each port in the optimal efficiency configuration. We then adjusted the excitation coil couplings until we reached the right impedance for each port. Once the circuit was in the optimal configuration, we recorded the scattering parameters.

### 5.4 Efficiency

The network analyzer displayed a smith chart showing each scattering parameter, which allowed us to tune and adjust the circuit in real time. Once we adjusted the circuit for optimal power transfer, we recorded the scattering parameters. The total efficiency is given by:  $\eta = |S_{12}|^2 + |S_{13}|^2$ . We measured this efficiency for various separations between the source and the two devices.

## 5.5 Effects of Parasitic Capacitance

In the course of our experiment, we encountered two peculiar phenomena. After careful study, we were able to determine the causes of these strange behaviors and eliminate them, which greatly improved the efficiency of our power transfer. Figure 5-4 shows a schematic depiction of the network analyzer, coaxial cable, excitation coil, and resonator, along with parasitic capacitances. We were able to determine that these parasitic capacitances were the cause of the strange phenomena which we observed.

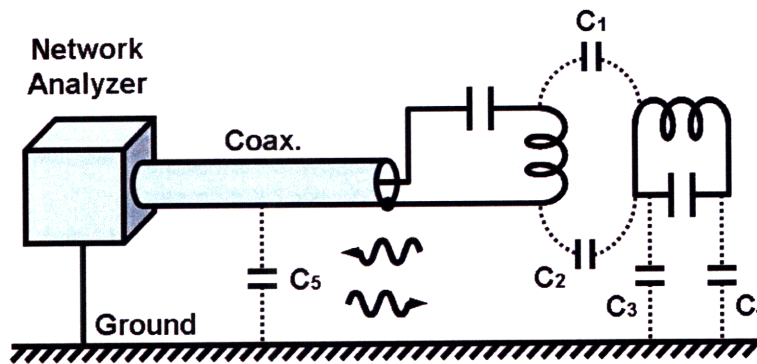


Figure 5-4: Schematic depiction of the parasitic capacitances.

The first strange behavior was the following: When we placed an excitation coil along the axis of a helical resonator, we found that the coupling would be strong in one orientation, but it would be weak when the excitation coil was rotated by  $180^\circ$ . We determined that this effect was caused by the parasitic capacitance,  $C_1$ . This capacitor creates an electric coupling between the excitation coil and the resonator which adds to the magnetic coupling. When the coil is rotated by  $180^\circ$ , the magnetic coupling coefficient changes sign, but the electric coupling remains the same. Therefore, the two effects add in one orientation, and subtract in the other, giving rise to the different coupling coefficients observed for the two orientations.

We were able to verify that  $C_1$  was the cause of this effect by placing a shield of copper tape around the excitation coil. This blocked the parasitic capacitance, and the coupling constant was nearly the same for both orientations. Once we determined the cause of this effect, we decided that it had no effect on our system's efficiency, and could therefore be safely ignored.

However, the second strange behavior which we observed did significantly impact

our system's efficiency. We observed that the tuning of our resonators was shifted whenever we moved the coaxial cables which connected to the excitation coils. We determined that this effect was caused by the parasitic capacitance,  $C_2$ . This capacitor allows the oscillating voltage on the resonator to excite waves along the outer conductor of the coaxial cable and the ground plane, which together behave like a transmission line.

The capacitor  $C_5$  represents the extra capacitance of a patch of the cable which is laying on the floor. We found that this capacitance presented enough of an impedance discontinuity to reflect the waves. We placed a ferrite ring around the coaxial cable before and after this discontinuity, and we found that it absorbed power when placed to the right of  $C_5$  (as shown in the schematic) and it had no effect when it was placed to the left of  $C_5$ . However, when we lifted the cable off the floor, the ferrite ring absorbed power, regardless of its location.

This implied that the resonator was losing power by setting up oscillations along the outer conductor of the coaxial cable. Unfortunately, unlike the case of  $C_1$ , it is very difficult to shield  $C_2$  in a way which does not itself decrease the Q of the resonator.

However, after discussing various methods of eliminating this problem, we eventually developed a solution using symmetry. We repositioned the excitation coil to hang beneath the helical resonator as shown in Figure 5-1, and as can be seen in the photograph in Figure 5-2. By symmetry, the excitation coil is equally far from both sides of the helical resonator, and therefore each end of the resonator has equal parasitic capacitance to the excitation coil. Because of this symmetry, any wave excited by one end of the helical resonator is exactly canceled by a wave excited by the opposite end. Furthermore, the electric dipole interaction between the excitation coil and the helical resonator is zero by symmetry. Therefore, this new arrangement eliminated both effects. With a 2m distance between the source and the devices, we observed an increase in efficiency from 50% to 57% after making this change.

The only drawback was that the mutual inductance between the excitation coil and the helical resonator is somewhat reduced because the excitation coil captures less flux in its new position. However, we found that the range of the coupling constant was still sufficient to achieve the correct impedance matching.



# Chapter 6

## Results 1

The following figures show the measurements made for the first experiment.

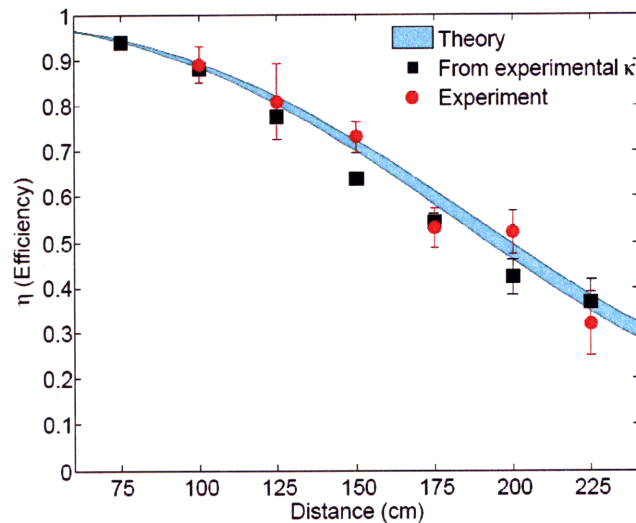


Figure 6-1: Efficiency as a function of distance between the two coils.

Based on the resonator parameters, and their uncertainties, our theoretical model predicted a resonant frequency of  $10.56 \pm 0.3$  MHz. The observed resonant frequency was 9.90MHz, which differed from the predicted frequency by 5%.

Our model also predicted a Q of about 2500, but the observed Q was  $950 \pm 50$ . This large discrepancy may have been caused by environmental factors, or it may be due to oxidation on the surface of the copper. Because of this large discrepancy, we inserted the experimentally measured Q into all of our other theoretical predictions. The widths of the theory curves reflect the uncertainty in the experimentally measured Q.

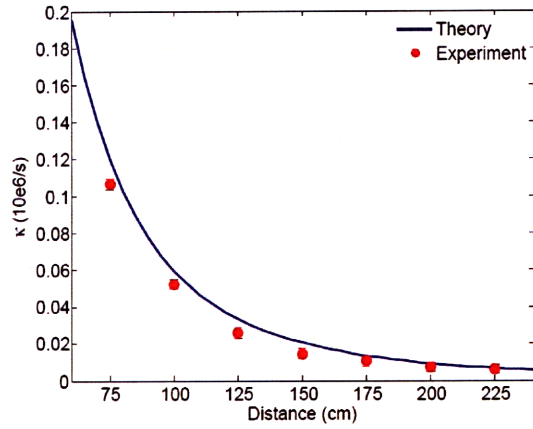


Figure 6-2: Coupling constant as a function of distance between the two coils.

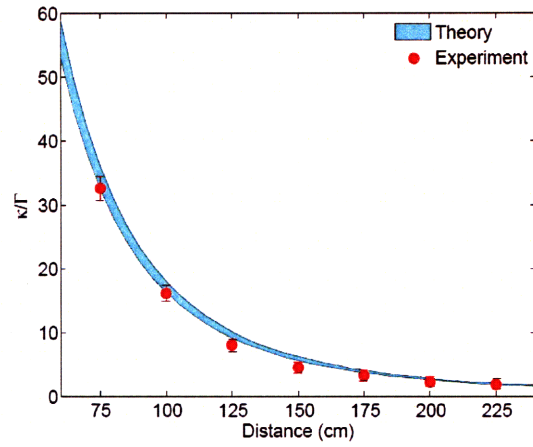


Figure 6-3: Strong coupling parameter as a function of distance between the two coils.

# Chapter 7

## Results 2

The following figures show the measurements made for the second experiment. The optimal efficiency shown in Figure 7-1 is a theoretical quantity calculated from the measured Q's and coupling constants of all of the resonators. The measured efficiency becomes lower than the optimal value if the system is detuned, or mismatched. Our data show that the measured values and the optimal values were all the same to within experimental error, which means that our system was correctly tuned and matched.

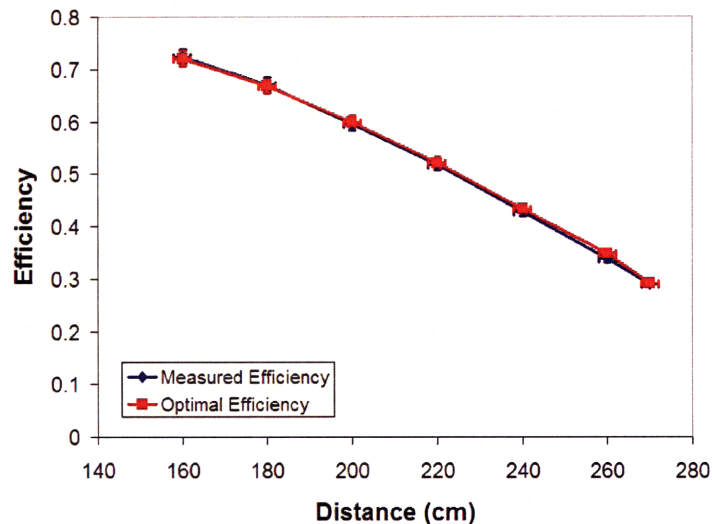


Figure 7-1: Total efficiency of power transfer from source to both devices.

Figure 7-3 shows the Q factors of the coils, which were determined by curve fitting in Matlab. The data marked “Dev. 1” was collected using only the Source & Device 1

Distance (cm)	Total Efficiency
160	72%
180	67%
200	60%
220	52%
240	43%
260	34%
270	29%

Table 7.1: Total efficiency of power transfer from source to both devices.

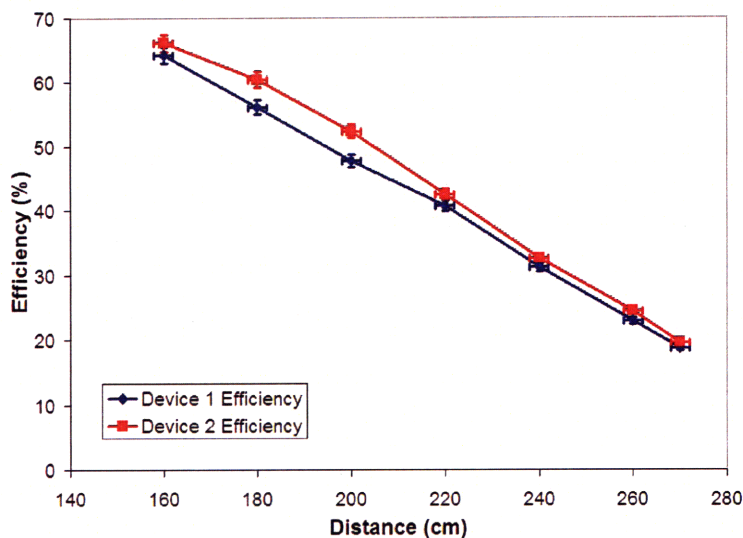


Figure 7-2: Efficiency comparison between the two device coils. These measurements were taken between the source and device 1 only, or between the source and device 2 only.

pair of resonators, and the data marked “Dev. 2” was collected using only the Source & Device 2 pair of resonators. The Q values are supposed to be constants, which means that the variations are caused by measurement error, or else by environmental effects. During the course of our measurements, the coils were shifted to various locations in the room, which could have affected their Q, especially the sensitive high-Q device coils. We also observed that the Q’s could rarely be measured to an accuracy greater than 5%. The average Q’s are about 800 for the source, and 1800 for the two devices.

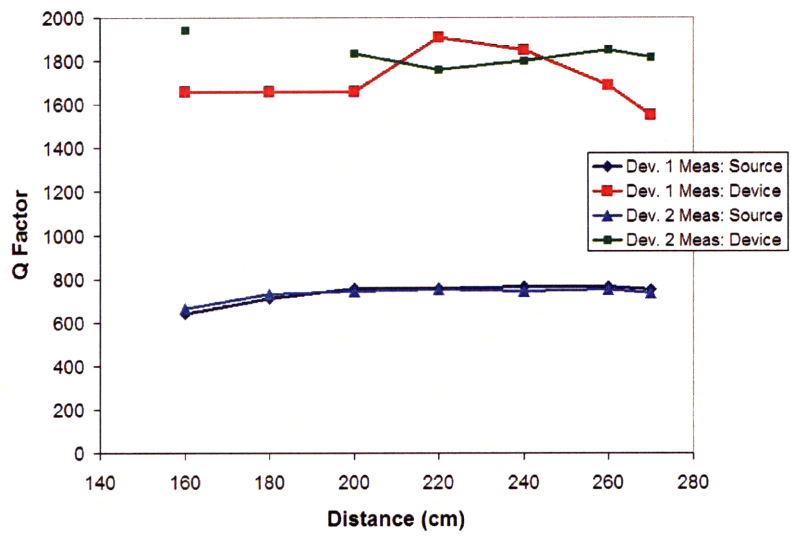


Figure 7-3: Q measurements of device and source coils.



# Chapter 8

## Conclusion

The results of our two experiments agreed well with our theoretical models, and they also met the design goals which we set for ourselves. The greatest discrepancy between our theoretical predictions and our measurements occurred in the values of the Q factors. Some possible causes for this discrepancy could be contamination of the copper surface, or interactions with metal objects in the room.

Our system of wireless power transfer shows great promise for practical applications, especially if the resonators are designed to incorporate automatic tuning and impedance-matching control. Furthermore, if efficiencies lower than 50% are acceptable, the necessity of fine-tuning and perfect matching becomes less essential, and the system can be quite robust against extraneous perturbations, as Figure 4-2 shows.

Other goals which remain for our project are to shrink the size of the device coils so that they can be incorporated in small, portable electronic devices. If this can be accomplished, then we might expect to see wirelessly powered electronics in the near future.





# Bibliography

- [1] N. Tesla, Apparatus for transmitting electrical energy, US patent number 1,119,732, issued in December 1914.
- [2] Kurs, et al. *Wireless Power Transfer via Strongly Coupled Magnetic Resonances* (Science, Vol. 317, July 6, 2007)
- [3] Kurs, Andre. *Power Transfer through Strongly Coupled Resonances* (Massachusetts Institute of Technology, September 2007)
- [4] A. Karalis, J. D. Joannopoulos, M. Soljacic, *Efficient Wireless Non-Radiative Mid-Range Energy Transfer* (Annals of Physics, 2007)
- [5] Kompfner, Rudolf. *Travelling-wave tubes* (Reports on Progress in Physics, 1952)
- [6] W. A. Edson, *Vacuum-Tube Oscillators* (Wiley, New York, 1953).